PVP - Vol. 63

Flow-Induced Vibration of Circular Cylindrical Structures - 1982 -

PVP - Vol. 63

Flow-Induced Vibration of Circular Cylindrical Structures

- 1982 -

presented at

THE PRESSURE VESSEL AND PIPING CONFERENCE
ORLANDO, FLORIDA
JUNE 27 – JULY 2, 1982

sponsored by

THE OPERATIONS, APPLICATIONS AND COMPONENTS COMMITTEE
PRESSURE VESSEL AND PIPING DIVISION, ASME

edited by

S. S. CHEN
ARGONNE NATIONAL LABORATORY
ARGONNE, ILLINOIS

M. P. PAIDOUSSIS
McGILL UNIVERSITY
MONTREAL, QUEBEC, CANADA

M. K. AU-YANG
BABCOCK AND WILCOX
LYNCHBURG, VIRGINIA

THE AMERICAN SOCIETY OF MECHANICAL ENGINEERS
United Engineering Center 345 East 47th Street New York, N. Y. 10017

Library of Congress Catalog Card Number 82-71617

FOREWORD

Circular cylindrical components have been extensively used in various mechanical and structural systems. Frequently, these components are submerged in flow, and may also convey or contain fluid. Therefore, they are susceptible to flow-induced vibration. Depending on the arrangement of these system components, the flow field, and other related parameters, systems consisting of circular cylindrical components may be subjected to small subcritical vibration as well as to large-amplitude fluidelastic instability. In the design of these components, the response to flow excitation is needed to ensure that the design life of the system will not deleteriously be affected by flow-induced vibration.

The purpose of this symposium is to provide a forum for the exchange of information among researchers and designers working in this field, as well as to contribute to the state of the art. Sixteen papers are presented covering a wide range of topics: single- and two-phase flows, axial and cross flow, single and multiple cylinders, flow-induced and acoustic excitations, subcritical vibration, dynamic instability, flow-field characterization, and structural response. These papers may be grouped in the following four categories.

1. Fluid-force Characterization for Circular Cylinders in Fluid

Fluid forces acting on a cylinder may be divided into fluid excitation forces, which are independent of structural motion, and motion-dependent fluid forces, which are functions of structural acceleration, velocity, and displacement. Four papers in this group characterize the fluid forces under different conditions. Hara and Kohgo report on an experimental study of a tube vibrating in an air-water mixture flow. Motion-dependent fluid forces include fluid inertia and fluid damping; the magnitudes of these forces are determined in terms of the added mass coefficient and modal damping ratio as functions of fluid void fraction. The fluid excitation force in two-phase cross flow is measured by Hara for a single tube and by Nakamura for a tube array. Two-phase flow excitation forces are found to be significantly different from those of a single-phase flow for some ranges of parameters. Jendrzejczk and Chen present a technique for measuring the fluid excitation forces acting on a single tube, two tubes in tandem, and two tubes normal to flow; measurements are made in water flow. It is recognized that the crux of flow-induced vibration analysis is the determination of the fluid forces. These papers have provided some useful data, and much more is needed in the future.

2. Dynamic Instability of Tube Banks in Cross Flow

Stability of a tube bank in cross flow is one of the most practically important and technically interesting problems. In the last decade, many innovative studies have been published. Four papers focus on this problem. In Japan, Tanaka and his colleagues report on the motion-dependent fluid forces acting on a square tube array with a pitch-to-diameter ratio of 2.0. These fluid forces are then used to predict the critical flow velocity and are compared with experimental results. In a companion paper, Ohta et al. employ the measured motion-dependent fluid forces to calculate the critical flow velocity of practical system components using a standard modal-analysis approach. On this side of the ocean, Weaver and his colleagues in Canada study the same problem using a different approach. A theoretical model is developed from the principles of fluid mechanics and the theory of elasticity. The essential features of instability phenomena predicted by the model are, in general, in agreement with the experimental observations. In another paper, they examine the differences of instability phenomena in air and in water for a parallel triangular array

of tubes with a pitch-to-diameter ratio of 1.375. These papers cover the essential issues and provide some solutions to this interesting problem.

3. Axial Flow-induced Vibrational Response

Depending on the configuration, the flow may be classified as internal, external, or combined internal-external. Connors et al. present an experimental study of the motion-dependent fluid force of a square array in an external axial flow; they find that the fluid damping force, similarly to that for a single cylinder, increases with flow velocity. A theoretical and experimental study of the response of a BWR jet pump to turbulent pressure fluctuations is conducted by Nakao and Torres. The study uses random vibration theory as well as large flow test facility to test a full-scale model; this is one of the samples illustrating the application of FIV theory to a nuclear-reactor-system component. The other two papers focus on piping-system response associated with internal flow. Hiramatsu et al. measure the fluid force and the piping-system response; an analytical method is also presented for predicting the steady-state response. Axisa and Gibert report on a finite element method for predicting the transient response of piping containing compressible fluid, including the effect of nonlinearities. The method is applied to study the effect of a solium-water reaction in an LMFBR secondary loop.

4. Acoustoelastic and Fluidelastic Vibration

Interaction of an acoustic field with structural motion can be significant; the resultant oscillation is called acoustoelastic vibration. Schwirian et al. use a computer program to deal with the pump-induced acoustic pressure. Application of the program to a practical test loop is illustrated. Simmons and Baldwin consider the vortex-excited acoustic response of a relief valve. A preliminary design guide to avoid vortex-excited resonance is proposed. The other two papers in this group study the inertial effect of fluid on structures. Interaction of structural oscillations with fluid motion results in coupled vibration of a fluid/structure coupled system; this is called fluidelastic vibration. Planchard et al. study the medium consisting of a large number of tubes in quiescent fluid. A computational method based on the homogenization technique is proposed to determine the equivalent sonic velocity and the natural frequency in the composite medium. Sattinger conducts a scale-model test for a shell submerged in fluid, to demonstrate the scaling laws for fluid-structure systems.

These papers have covered several aspects of flow-induced vibrations. It is hoped that this volume will be useful to designers as well as researchers in this field. Certainly, many unresolved questions remain to be pursued and will hopefully continue to receive attention in the future. Readers who are interested in the general area of flow-induced vibration may also be interested in the following publications: "Flow Induced Vibrations," edited by S. S. Chen and M. D. Bernstein, ASME, 1979; and "Flow-Induced Vibration of Power Plant Components," edited by M. K. Au-Yang, ASME, PVP-41, 1980.

We wish to express our thanks to the authors for their cooperation in preparing their manuscripts and for their willingness to participate and share their experience with others at this symposium.

S. S. Chen
M. P. Paidoussis
M. K. Au-Yang

CONTENTS

ADDED MASS AND DAMPING OF A VIBRATING ROD IN A TWO-PHASE AIR-WATER MIXED FLUID

F. Hara, Associate Professor and **O. Kohgo**, Graduate Student
Tokyo University of Science
Tokyo, Japan

ABSTRACT

This paper presents the added mass and damping of a vibrating circular rod in a two-phase fluid. The experimental fluid added mass agrees well with the theoretical value. The fluid damping ratio, in general, increases linearly with the void fraction, but over a certain void fraction it decreases gradually with the void fraction.

INTRODUCTION

Two kinds of force act on a structure vibrating in a fluid--one proportional to the acceleration and the other proportional to the velocity. The first force generates added mass and the second damping coefficient, as coefficients to the acceleration and velocity. These two coefficients are essential to an evaluation of the response of a structure vibrating in a fluid.

Several papers on this problem have been confined to dealing with a single-phase fluid only. Chen[1] theoretically evaluated added mass and damping of a circular rod vibrating in a liquid, using a two-dimensional analysis of the incompressible, viscous fluid, giving experimental credibility to his theoretical analysis. Fujimoto [2] et al. clearly showed the dependence of these quantities on the vibrational amplitude of a rectangular rod immersed in water.

Two-phase fluid plays an important role in the utilization of industrial facilities such as steam generators and boiling water reactors. It is well known that a two-phase fluid flow generally exerts unexpectedly large forces on a structure immersed in such a flow[3]. Although added mass and damping due to the two-phase fluid must be correctly determined to evaluate the vibrational response of a structure in such a flow, few papers on this are yet available. Carlucci presented experimental data on added mass and damping of rod bundles in a still, two-phase fluid[4] as well as in a two-phase axial flow[5]. In his paper[4], however, the range of experimental conditions for rod-cylinder clearance was not wide enough, and the two-phase fluid configuration and bubble size were not clearly specified. At this point in research on this problem, then, more systematic experimental data on added mass and damping is needed with regard to two-phase fluid cases.

This paper presents experimental data on the added mass and damping ratio of a vibrating circular rod immersed in a two-phase fluid in an outer circular container. Six cases were tested for different clearances between the rod and container: the ratio $\gamma = D/d$ varies from 2 to 16, where D = the inner diameter of the container and d = rod diameter. It was found that added mass decreased linearly with an increasing void fraction up to about 40%. Over that value, however, it deviated greatly from the above-mentioned linear dependence on the void fraction. Damping increased almost linearly with the void fraction, which is similar to characteristics of the added mass. Over 40% of the void fraction, it became almost

independent of the air concentration in the two-phase fluid.

This paper also deals with the spring effect of an air bubble on added mass, explaining the peculiar dependence of added mass on the void fraction.

METHOD OF EVALUATING ADDED MASS AND DAMPING

Hydrodynamic Method

When a two-phase air-water fluid is assumed to be homogenous, incompressible, and inviscid, the two-dimensional hydrodynamic theory on added mass developed by Chen[1] gives the following formula for evaluating added mass per unit length ρ_a of a vibrating rod in a two-phase fluid, neglecting the density of air,

$$\rho_a = \left(\frac{\gamma^2 + 1}{\gamma^2 - 1}\right)(1-\alpha)\rho_w \quad , \gamma = D/d, \quad (1)$$

where ρ_w = water mass per unit length for the cross-sectional area $\pi d^2/4$, and α = void fraction.

Random Vibration Method

Applying the linear theory on lateral vibration of a slender rod to this problem, the equation of a rod in a two-phase fluid is easily described as

$$EI\frac{\partial^4 y}{\partial z^4} + K_a(z,\alpha)y + (C + C_a(z,\alpha))\frac{\partial y}{\partial t} + (\rho + \rho_a(z,\alpha))\frac{\partial^2 y}{\partial t^2} = W\,\delta(z-a) + T(z,\alpha). \quad (2)$$

In eq. (2), y is rod displacement, $K_a(z,\alpha)$ is the two-phase fluid induced spring effect, $C_a(z,\alpha)$ is two-phase fluid damping, $\rho_a(z,\alpha)$ is two-phase fluid added mass, a is the location of external excitation, and ρ is rod mass per unit length. On the right-hand side of eq. (2), W and T are external and two-phase fluid induced excitations. Since the second natural frequency is widely separated from the first, only the first vibration mode is considered. Vibration displacement y is given as follows:

$$y = X(z)Y(t), \quad (3)$$

where X(z) is the first normalized modal function such that $\int_0^1 X^2 dz = 1$, and Y(t) is a function of time. Substituting eq. (3) into eq. (2), multiplying X(z) with both sides of eq. (2), and integrating over rod length 1 yield

$$(M^* + M_a^*)\ddot{Y} + (C^* + C_a^*)\dot{Y} + (K^* + K_a^*)Y = W + T^*, \quad (4)$$

where

$$M^* = \rho l/X(a),$$

$$K^* = \lambda^4 EI/X(a),$$

$$C^* = Cl/X(a),$$

$$T^* = \int_0^1 TX dz/X(a),$$

$$M_a^* = \int_0^1 \rho_a X^2 dz/X(a),$$

$$K_a^* = \int_0^1 K_a X^2 dz/X(a),$$

$$C_a^* = \int_0^1 C_a X^2 dz/X(a),$$

and λ = the first eigen value.

Undamped natural frequency $f_n(\alpha)$ obtained from eq. (4) is

$$f_n(\alpha) = \frac{1}{2\pi}\sqrt{\frac{K^* + K_a^*}{M^* + M_a^*}} \quad . \quad (5)$$

Undamped natural frequency $f_n(\alpha)$ is almost equal to resonance frequency $f_r(\alpha)$ in eq. (4). It is then assumed that

$$f_n(\alpha) = f_r(\alpha). \quad (6)$$

In eq. (4), M_a^* and K_a^* must be zero for the case of void fraction $\alpha = 1.0$, i.e., in air. The f_n in air thus is

$$f_n(\alpha=1) = \frac{1}{2\pi}\sqrt{K^*/M^*} = f_r(\alpha=1). \quad (7)$$

From eq. (6) and (7),

$$M_a^* = \left\{\left(\frac{f_r(\alpha=1)}{f_r(\alpha)}\right)^2 \left(1 + \frac{K_a^*}{K^*}\right) - 1\right\} M^* \quad , (8)$$

or, multiplying X(a)/1 with both sides of eq. (8) and defining ρ_a^* as $\int_0^1 X^2 \rho_a dx/1$, then eq. (8) is rewritten as

$$\rho_a^* = \left\{\left(\frac{f_r(\alpha=1)}{f_r(\alpha)}\right)^2 \left(1 + \frac{K_a^*}{K^*}\right) - 1\right\}\rho \quad . \quad (9)$$

Assuming the statistical independence of white Gaussian excitation force W from two-phase fluid induced excitation force T* and T* as white Gaussian,

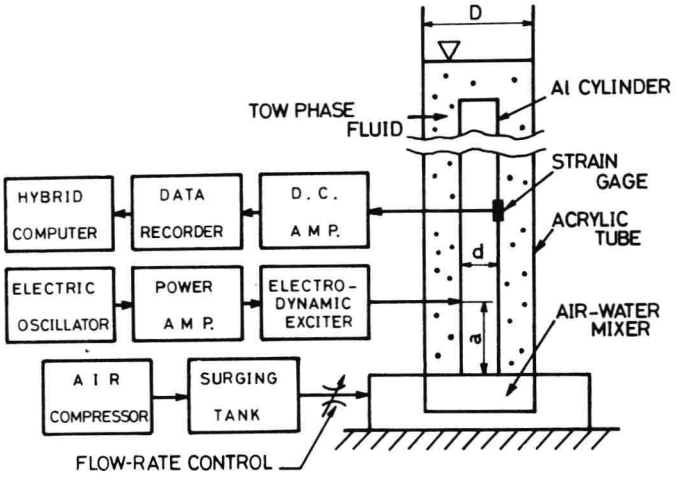

Fig. 1 Schematic diagram of experimental apparatus

complex compliance, H, can be defined as

$$H = \frac{1}{-(M^*+M_a^*)\omega^2+i(C^*+C_a^*)\omega+(K^*+K_a^*)} \quad (10)$$

The power spectral density (PSD) of displacement response $G_y(\omega)$ is obtained as

$$G_y(\omega) = |H|^2 (G_w(\omega) + G_{T^*}(\omega)) \quad (11)$$

Since G_w and G_{T^*} are constant, total camping ratio ζ_t is evaluated from PSD $G_y(\omega)$ as

$$\zeta_t = 1/2\sqrt{N-1} \times \Delta f/f_r(\alpha), \quad (12)$$

where Δf is a 1/ N peak band width for the first mode vibration in $G_y(\omega)$. As total damping ratio ζ_t is theoretically obtained from eq. (4) as

$$\zeta_t = \frac{C^* + C_a^*}{2\sqrt{(M^* + M_a^*)(K^* + K_a^*)}} \quad (13)$$

and $C^* = 2\zeta_t(\alpha=1)\sqrt{M^*K^*}$ for $\alpha = 1.0$, i. e., in air, two-phase fluid damping ratio ζ_a becomes

$$\zeta_a = \zeta_t(\alpha) - \frac{\zeta_t(\alpha=1)}{\sqrt{(1+M_a^*/M^*)(1+K_a^*/K^*)}} \quad (14)$$

Finally, if spring effect K_a^* of the two-phase fluid is neglected, added mass ρ_a^* and two-phase fluid damping ratio ζ_a are evaluated by the following equations,

$$\rho_a^* = \left\{\left(\frac{f_r(\alpha=1)}{f_r(\alpha)}\right)^2 - 1\right\}\rho, \quad (15)$$

$$\zeta_a = \zeta_t(\alpha) - \zeta_t(\alpha=1)/\sqrt{(1 + \rho_a^*/\rho)}. \quad (16)$$

EXPERIMENTAL APPARATUS AND PROCEDURES

Figure 1 shows a schematic diagram of the experimental system in which a circular aluminum rod with a diameter, d, of 5 mm, and 500 mm long, was concentrically installed in an acrylic outer circular container. One end of the rod was fixed at the bottom part, which worked as an air injector. The injector consisted of two circular disks, the upper having 0.1 mm holes every 4 mm in a grid fashion and the lower having 2 mm holes with 4 mm pitches for both directions. The inner diameter of the outer container was 80, 50, 40, 30, 20, or 10 mm.

The test rod was excited by an electrodynamic exciter, W, at a point 38 mm from the fixed end, and input to the exciter was white Gaussian random. The vibrational strain of the rod was measured 50 mm from the fixed end.

Water filled the container to a certain height, h_w, then air was injected into the water from the air injector in the form of air bubbles to raise water height to 540 mm from the container bottom. Thus, void fraction α in the container was evaluated by the formula $1-h_w/540$.

Table 1 shows void fraction α and ra-

Table 1 Experimental conditions specified by void fraction α and gap ratio γ = D/d

γ \ VOID FRACTION α %	0	5	10	20	30	40	50	60	70
16		B	B	B	B	B	B	B	B
10		B	B	B	B	B	B	B	
8		B	B	B	B	B•S			
6		B	B	B	B	B•S			
4		B	B	B	B	B•S			
2		$S^{7.5}$	S^{15}	S	S	F	F	F	F

B:BUBBLE S:SLUG F:FROTH

tio γ = D/d, with two-phase fluid configurations; B = bubble, B + S = bubble + slug, S = slug, and F = froth. Photo 1 shows these typical fluid phase configurations.

Vibrational strain signals obtained from the strain gage on the rod surface 50 mm from the fixed end were digitized by an A-D converter with a sampling period of 0.02 s, and their PSDs were numerically calculated using 5,000 digits. For each experimental condition in Table 1, five PSDs were calculated and their average obtained at each frequency. After averaging, a migrating average was applied to the PSD distribution to find a clearcut peak in the PSD.

RESULTS

Vibrational Strain PSDs

Figures 2(a) to (h) are typical PSDs of vibrational strains produced on the rod surface through white Gaussian random force W and by two-phase fluid induced random force T. Figures (a) to (d) are for cases of γ = 10; (a) is for α = 100%, i.e., in air; (b) for α = 0%, i.e., in water; (c) for α = 30%; and (d) for α = 60%. Increasing the void fraction, the peak PSD frequency rose and the distribution became wider. Figures (e) and (f) are for γ = 4; (e) is for α = 0% and (f) for α = 30%. Figures (g) and (h) are for γ = 2; α = 0% and α = 30%. Decreasing γ for α = 0%, the peak frequency became smaller, meaning that, in water, added mass increased with the decrease of the gap between the vibrating rod and the outer wall. For α = 30%, i.e., in two-phase fluid, this decrease in PSD peak frequency, although not so clear, was recognizable,

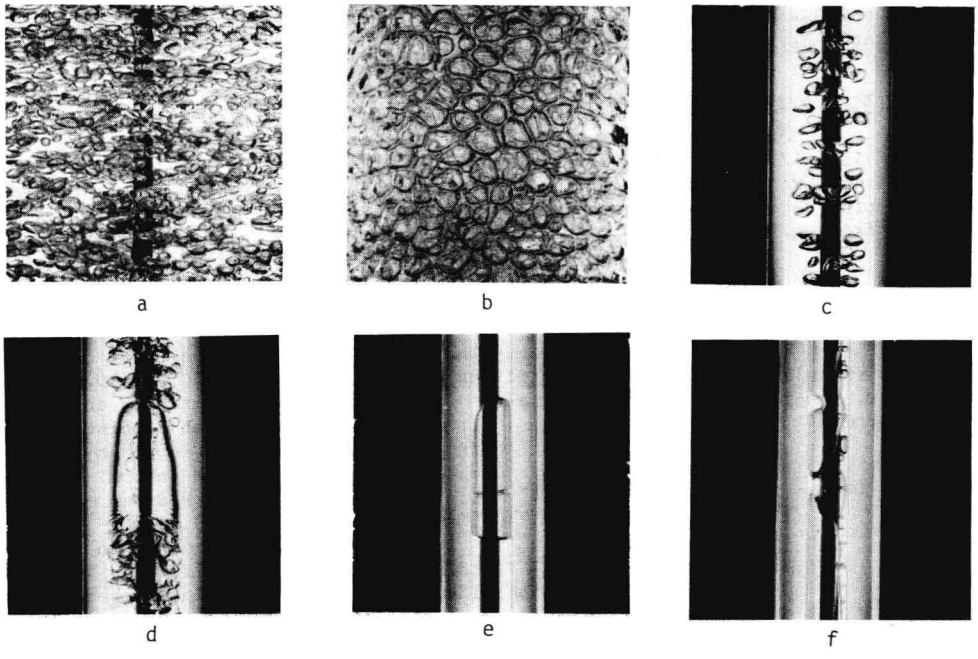

Photo 1 Typical two-phase fluid configurations, (a) γ = 16, α = 10%, bubble, (b) γ = 16, α = 70%, bubble, (c) γ = 4, α = 10%, bubble, (d) γ = 4, α = 40%, bubble + slug, (e) γ = 2, α = 15%, slug, (f) γ = 2, α = 50%, froth

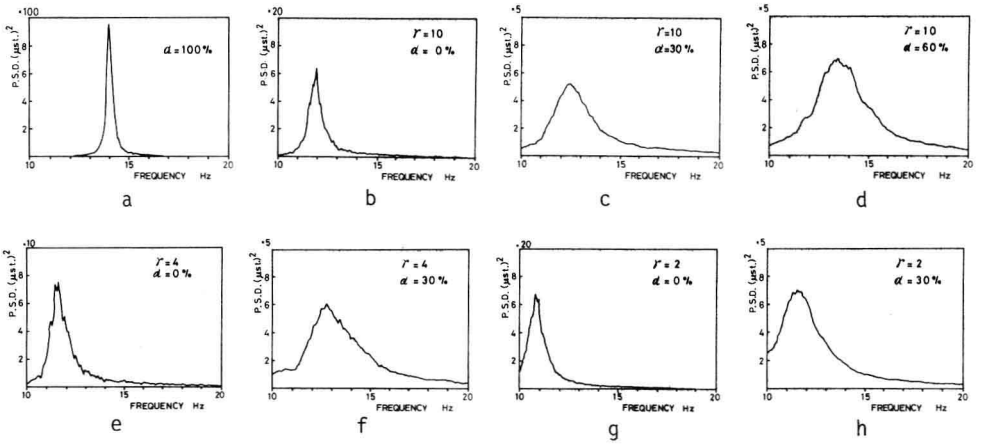

Fig. 2 Examples of typical PSD of vibrational strains produced on the test rod surface

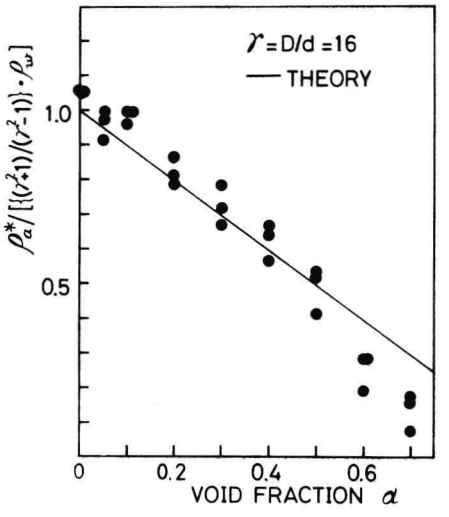

Fig. 3 Added mass ρ_a^* and void fraction α for γ = 16 (— THEORY in eq. (1))

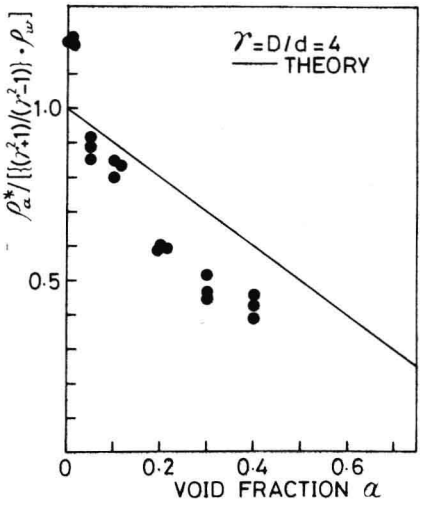

Fig. 4 Added mass ρ_a^* and void fraction α for γ = 4 (— THEORY in eq. (1))

as Figs. (c) and (h) show. From these general observations, it can be qualitatively said that two-phase fluid added mass decreases and damping increases with the void fraction.

Added Mass

Figure 3 shows normalized added mass $\rho_a^*/\{(\gamma^2+1)/(\gamma^2-1)\}\rho_w$ vs void fraction α for γ = 16. Here, ρ_a^* was evaluated from eq. (15). The solid line indicates ratio ρ_a in eq. (1) to $(\gamma^2+1)/(\gamma^2-1)\cdot\rho_w$, i.e., $1-\alpha$. In the range of void fraction 0% to 50%, added mass ρ_a^* agreed well with the theoretical one calculated from eq. (1). For $\alpha \geqq 50\%$, however, added mass deviated from the theoretical trend, showing smaller values. Almost the same feature was found for γ = 16, 10, 8, and 6. For γ = 4, added mass of the two-phase fluid showed a value smaller than the theoretical one, even in the range of small void fractions (Fig. 4). For an even smaller gap of γ = 2, added mass showed a value almost equivalent to the theoretical one in the range of void fractions smaller than α = 40%. For $\alpha > 40\%$, however, added mass was drastically smaller

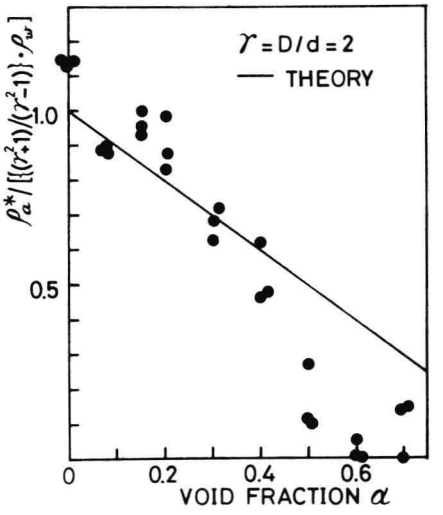

Fig. 5 Added mass ρ_a^* and void fraction α for γ = 2 (— THEORY in eq. (1))

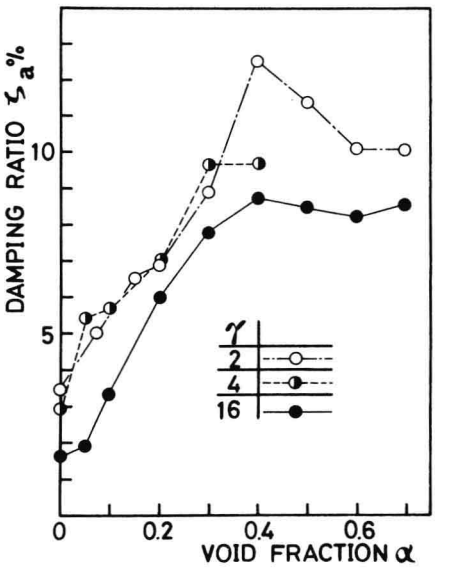

Fig. 7 Damping ratio ζ_a and void fraction α

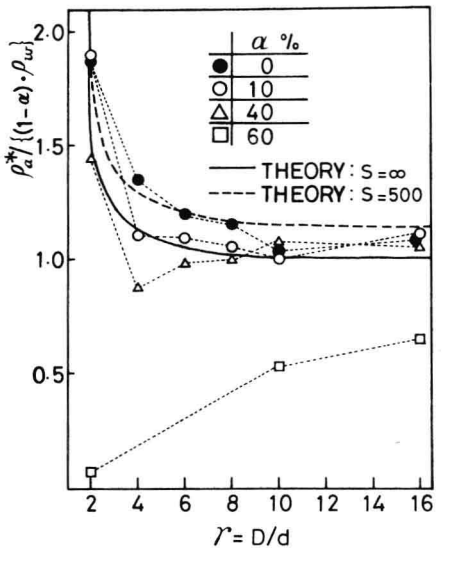

Fig. 6 Added mass ρ_a^* and γ (S = ∞: inviscid, S = 500: viscous fluid (water))

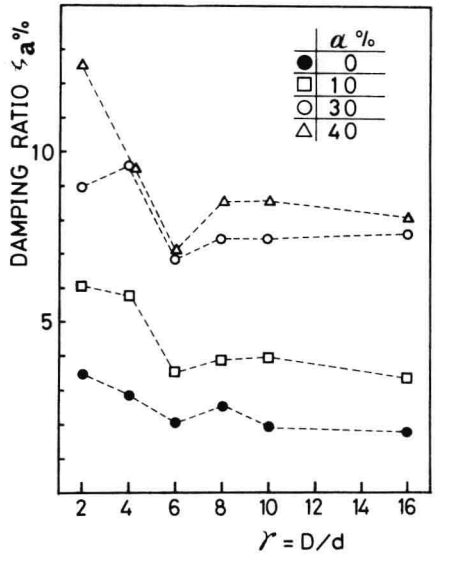

Fig. 8 Damping ratio ζ_a and γ

than the theoretical one, 1 - α (Fig. 5).

Figure 6 shows the ratio of added mass ρ_a^* to (1 - α) ρ_w and gap ratio γ. This figure indicates that, for smaller void fractions, experimental added mass from eq. (15) showed rather good agreement with the theoretical one (eq. (1)). For large void fractions α > 40%, added mass showed a much smaller value than the theoretical one for all γ in the experiments.

Damping Ratio

Figure 7 shows two-phase fluid damping ζ_a (%) evaluated from eq. (16) as a function of void fraction α. For each γ, damping ratio ζ_a increased almost linearly with the void fraction up to α =40%,

then decreased gradually for further increases of void fraction.

Figure 8 shows the effect of γ on two-phase fluid damping ζ_a. For smaller void fractions, ζ_a increased as γ decreased. In higher void fractions, however, this trend was somewhat disturbed due to two-phase fluid configurations.

DISCUSSION AND CONCLUSIONS

Added mass and damping obtained experimentally are interpreted as vibrational system parameters for the first vibration mode of a cantilever-type rod in the two-phase fluid. It should be noted here, then, that the value of these determined experimentally has the possibility of being dependent on the vibrational configuration of the rod and also on the order of the vibration.

Extending the method of evaluating added mass and damping through random vibration technique to higher vibration mode cases, it may be possible to obtain the distribution of added mass and damping along the rod axis, $\rho_a(z,\alpha)$ and $C_a(z,\alpha)$. However, this is work to be done in future.

Carlucci[5] pointed out two mechanisms for reducing two-phase fluid added mass, one being nonhomogeneity of bubble configuration in the mixed fluid and the other being the spring effect of the two-phase fluid on the rod vibration system. Thus, the discussion here focuses on the two points in relation to added mass.

Nonhomogeneity Effects

Comparing vibrational rod dimensions in axial and radial directions with bubble size in the two-phase fluid, the nonhomogeneity effect is assumed to appear in cases where the rod diameter or length is smaller than bubble size. Thus the homogeneity of the two-phase mixed fluid may be directly related to bubble configuration in a macroscopic sense as well as with local void fraction distribution in a microscopic sense. In Fig. 3 and 5, the experimental value of added mass evaluated by eq. (15) agreed with the theoretical one for bubble and slug configurations, but for froth configuration in $\gamma = 2$, the deviation of experimental added mass is large, meaning the amount of liquid existing at the outer wall could reduce the added mass to the marked degree shown in Fig. 5.

Even in a mixed bubble fluid configuration, however, added mass was rather small in higher void fractions or at $\gamma = 2$. This discrepancy between experimental and theoretical values indicates other mechanisms of reducing two-phase fluid added mass, such as the nonhomogeneity of local void fractions or the spring effect of the two-phase fluid.

Table 2 Two-phase fluid spring effect and added mass modification

γ	α (%)	K_a^*/K^*	Added mass		
			eq.(15)/eq.(1)	eq.(9)/eq.(1)	eq.(9)/eq.(15)
4	10	0.0662	0.9169	1.152	1.25
4	30	0.0119	0.7814	0.8312	1.06
16	20	0.0324	1.0526	1.1952	1.14
16	60	0.0148	0.6865	0.7958	1.16

Spring Effect

The calculated peak value of compliance $|H|^2$, by using the total damping ratio $\zeta_t(\alpha)$ determined from eq. (12) and rod stiffness K*, gave a recognizable discrepancy from the peak value of experimental compliance, implying the existence of spring effect on experimental compliance. Further, bubbles between the vibrating rod and the inner wall of the container might be deformed by rod motion. This deformation would generate a repulsive force against the rod which might play a role in effects on the rod vibration in the two-phase fluid.

When taking into account the spring effect of two-phase fluid in evaluating added mass, the increase of added mass is easily calculated from eq. (9) for experimental value $\{f_r(\alpha=1)/f_r(\alpha)\}^2$ as

$$\Delta\rho_a = \left\{\frac{f_r(\alpha=1)}{f_r(\alpha)}\right\}^2 \frac{K_a^*}{K^*}\rho . \quad (17)$$

Since K_a^* must be positive, $\Delta\rho_a > 0$, so if a spring effect existed, the added mass must be larger than the experimental ones obtained from eq. (15) in the previous section.

To evaluate two-phase fluid spring effect K_a^*, the magnitude of compliance $|H|^2$ was experimentally obtained for the two cases of single-phase water and two-phase fluid with void fraction α. From peak values in $|H|^2$ for both cases, K_a^* was easily evaluated using total damping ratio ζ_t. Table 2 shows results for $\gamma = 4$ and 16. Table 2 also indicates that a two-phase bubble fluid could produce only a small spring effect (1 to 6% for rod stiffness), but that the spring effect greatly influenced added mass. For higher void fractions, e.g., $\alpha = 30\%$ at $\gamma = 4$ or $\alpha =$

60% at γ = 16, experimental added mass, including the two-phase fluid spring effect, shows a still smaller value than the theoretical one, indicating that the microscopic nonhomogeneity in local void fraction might be effective in reducing added mass. There also might exist the possibility of affecting the magnitude of added mass--e.g., the effective axial flow component of the rod surface or change of mode shape of the cantilever-type rod. These, however, have not been examined here.

In conclusion, this paper presented experimental values for added mass and damping of a vibrating rod in a mixed air-water two-phase fluid for a wide range of void fractions and of rod-container clearance, leading to the following conclusions.

(1) Added mass decreased linearly with the increase of void fraction in the range of small void fraction, but it became drastically small for higher void fractions.

(2) Corresponding to the added mass character in (1), two-phase fluid damping increased linearly with void fractions up to α = 40%. It decreased gradually, however, with α for $\alpha > 40\%$.

(3) We discussed three kinds of mechanisms reducing two-phase fluid added mass so much in higher void fractions, i.e., the macroscopic nonhomogeneity of bubble configuration in the fluid; the microscopic mechanism of local void fraction; and the spring effect of the two-phase fluid.

(4) The spring effect was quantitatively evaluated, offering an approximately 6 to 25% increase in added mass.

ACKNOWLEDGMENTS

The authors wish to express their gratitude to Messrs. N. Ogawa (graduate student, Tokyo University of Science) and H. Kajiwara (undergraduate student, Tokyo University of Science) for their assistance in experimental work.

REFERENCES

1. Chen, S. S., et al., "Added Mass and Damping of a Vibrating Rod in Confined Viscous Fluids," ANL-CT-75-08, 1974, pp. 1-25.

2. Fujimoto, S., et al., "Fluid Damping of a Vibrating Rectangular Rod in a Confined Fluid," JSME Preprint, No. 810-3, 1981, pp. 130-131.

3. Hara, F., "Two-phase Cross-flow Induced Vibrations in a Circular Cylinder (Lift and Drag Forces)," JSME Preprint, No. 810-16, 1981, pp. 1-7.

4. Carlucci, L. N., "Hydrodynamic Mass and Fluid Damping of Rod Bundles Vibrating in Confined Water- and Air-water Mixtures," Trans. 4th SMiRT, Vol. D, D3/11, 1977, pp. 1-10.

5. Carlucci, L. N., "Damping and Hydrodynamic Mass of a Cylinder in Simulated Two-phase Flow," ASME Journal of Mechanical Design, Vol. 102, 1980, pp. 597-602.

TWO-PHASE CROSS-FLOW-INDUCED FORCES ACTING ON A CIRCULAR CYLINDER

F. Hara
Department of Mechanical Engineering
Tokyo University of Science
Tokyo, Japan

ABSTRACT

This paper clarifies experimentally the characteristics of unsteady flow-induced lift and drag forces acting on a circular cylinder immersed perpendicular to a two-phase bubbly air-water flow, in conjunction with Karman vortex shedding and pressure fluctuations.

INTRODUCTION

Karman vortex shedding and fluid elastic excitation are well known causes of violent oscillation in a cylinder or tube array immersed in a single-phase cross flow. Connors[1], Chen[2], Pettigrew[3], Blevins[4], and others have published many papers on this problem. Several situations exist in our technological field, however, where two-phase fluid (e.g., a liquid-gas mixture) plays an inevitable role in the use of facilities such as steam generators, condensors, and boiling water reactors. Shin and Wambsganns[5] showed an actual tube failure in a steam generator tube bank apparently caused by two-phase flow-induced vibration.

Two-phase air-water or steam-water flow-induced vibrations (hereafter, FIV) thus present a new side of on-site FIV problems, although among the very few research works done are those by Pettigrew et al.[6], and Heilker and Vincent [7], and increasing attention is being paid to FIV problems with regard to safe operation of heat exchangers or steam generators.

To understand the actual two-phase cross-flow induced vibration mechanism in tube bank systems, and to develop the technological means to suppress such vibrations, experimental work is needed. We initially utilize the very simplest case--that of a single cylinder immersed perpendicular to the flow--for a fundamental and academic work on unsteady fluid forces acting on a single cylinder in a two-phase bubble cross flow, i.e., we experimentally examined (1) Karman vortex shedding and pressure fluctuations and (2) two-phase flow-induced unsteady lift and drag forces with regard to flow velocity, air concentration, and bubble size. Experimental results presented here show that Karman vortex shedding disappears over a certain value of air concentration in the two-phase flow and, related to this disappearance, two-phase flow-induced lift and drag forces show interesting characteristics in frequency and magnitude. That is, flow-induced forces are rather small and periodical in low air concentration but become very large and random in higher air concentration.

EXPERIMENTAL PROCEDURES

Two-phase Flow Test Loop

The two-phase air-water flow loop used for the experiments in this paper was designed to produce a steady flow in the test section through a 1.5 m water head. From an upper constant level tank, water flowed down to a water tank through an orifice and a flow rate control valve. The water flow rate, Q_w (m^3/s), measured by the orifice, was in-

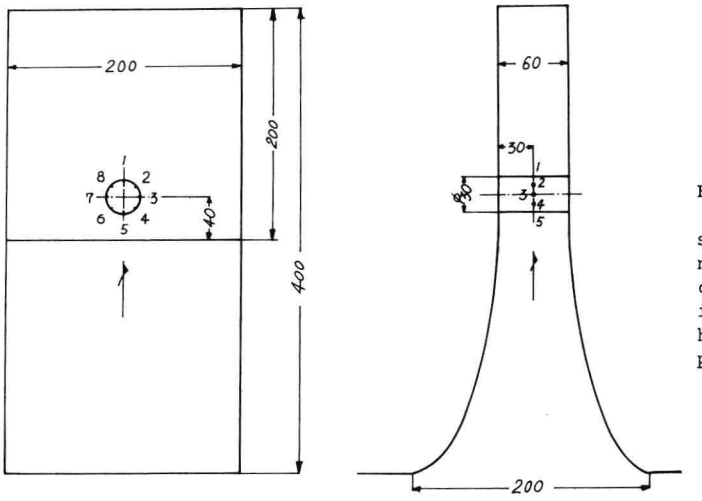

Fig. 1 Details of the rectangular shaped test section, nozzle, and 30 mm test cylinder, where numbers indicate 1 mm diameter holes for measuring pressure fluctuations

dicated on a manometer. The upper tank kept a constant water head through water overflowing to a lower buffer tank. Water in the water tank flowed up to a nozzle connected to a 200 mm x 60 mm test section, and was there accelerated to a specified velocity at the test section entrance. Air, pressurized to about 0.2 MPa, went to an accumulator, then reached an air flow meter through a flow rate control valve. Air pressure was measured at the flow meter exit. Air was injected through an air injector with 1 mm diameter holes into almost still water 0.3 m below the nozzle entrance, producing medium-sized air bubbles (about 20% of the test cylinder's diameter (30 mm)). Air and water were mixed into a homogeneous two-phase fluid in the nozzle, then entered the test section. A 30 mm circular test cylinder was installed at the center line 40 mm downstream from the nozzle exit. After passing the cylinder, the two-phase fluid went to a lower constant head tank. Air was then released into the atmosphere, and water overflowed the tank, returning to the buffer tank. A pump raised the water in the buffer tank to the upper constant head tank.

Figure 1 details the rectangular test section (200 mm x 60 mm) and the nozzle, whose entrance area was 200 mm x 200 mm and height 200 mm. The nozzle exit area was 200 mm x 60 mm; two of the nozzle walls formed an elliptic curve, while the other two were flat. The maximum water flow velocity available in the test section was 0.6 m/s, corresponding to Reynolds number = 1.8×10^4 for a representative fluid mechanical length of 30 mm (the cylinder diameter). The flatness of water velocity distribution was $\pm 1\%$ for an average flow velocity of 0.4 m/s at a section 40 mm downstream from the nozzle exit. The homogeneity of the two-phase flow was tested through void fraction distribution measured by a needle-type electric void probe over the cross-section (200 mm x 60 mm) at the same location as above. Results were completely satisfactory, indicating a $\pm 1.5\%$ variation. Figure 1 also shows the location of pressure taps (numbered 1 to 8)--equally spaced 1 mm diameter holes along circumferences at the circular cylinder's mid section for measuring pressure fluctuation.

Figure 2 shows a test cylinder for the measurement of unsteady lift and drag forces using cross-configurated flat springs, each of which detected a lift or drag force component. The natural frequency of the cylinder-spring system was about 100 Hz in each direction, which was sufficiently large compared to the dominant frequency of unsteady two-phase flow induced forces.

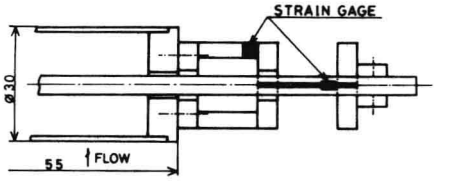

Fig. 2 30 ø test cylinder for flow-induced-force measurement

Instrumentation and Data Processing

Pressure Fluctuations. Two-phase flow-induced pressure fluctuations were simultaneously measured at points 1 and 5, 2 and 6, 3 and 7, and 4 and 8 on the cylinder (Fig. 1). The electrical output signals of pressure fluctuations from strain-gage-type pressure transducers (Kyowa, PG-200 GD) were amplified by Kyowa DPM-11013 amplifiers and recorded on magnetic tape. They were converted to digital form by an A-D converter with a sampling period of 0.025 second. The data number size was 2,000 digits. Using this digitized data, the power spectral density (PSD) and root mean square (RMS) of differential pressure fluctuations were calculated for the experimental cases shown in Table 1.

Lift and Drag Forces. Unsteady lift and drag forces generated by the two-phase flow on the cylinder were detected as strain signals in the small flat springs attached at both ends of the cylinder (Fig. 2). Electrically amplified strain signals were recorded on magnetic tape. Lift and drag forces simultaneously measured for each experimental condition shown in Table 1 were also converted to digital form, with the same sampling period and data number size as cases for the pressure fluctuation experiment. The PSD, RMS, and correlation between unsteady lift and drag forces were numerically calculated.

Flow Visualization. At points 3 and 7 in Fig. 1, black ink was injected into the two-phase flow to yield a dark trail showing the wavy motion of wakes. Two-phase flow wake patterns were photographed to investigate Karman vortex shedding from the cylinder. The oscillatory motion of black ink trails behind the cylinder was detected by a CdS photodiode to measure Karman vortex shedding frequency.

Table 1 Experimental conditions specified by Q_w and Q_a

Q_a $\times 10^{-5}$ (m^3/s)	Q_w (m^3/s)					
	0.0012	0.0024	0.0036	*0.0048	0.0060	0.0072
0.0	0.0	0.0	0.0	0.0	0.0	0.0
18.8	0.135	0.072	0.050	0.038	0.030	0.025
38.2	0.241	0.137	0.096	0.074	0.060	0.050
*59.0	0.330	0.197	0.141	0.109	0.090	0.076
81.7	0.405	0.254	0.185	0.145	0.120	0.102
106.8	0.471	0.308	0.229	0.182	0.151	0.129
135.3	0.530	0.361	0.273	0.220	0.184	0.158
*168.4	0.584	0.412	0.319	0.260	0.219	0.190
191.5	0.615	0.444	0.347	0.285	0.242	0.210

Bubble Size. Air bubble diameters for both lift and drag force directions were measured from photos of the two-phase bubble flow for about 100 bubbles and the average value and standard deviation were evaluated.

Experimental Conditions

The two-phase flow condition was specified by water flow rate Q_w (m^3/s) and air flow rate Q_a (m^3/s), shown in Table 1, where an air concentration, α, defined as $Q_a/(Q_w + Q_a)$, is also described, ranging from 0.0 to 0.615. In Table 1, experimental series indicated by an asterisk (*) were omitted for the two-phase flow pressure measurement experiment. The Reynolds number calculated by VD_o/ν (V = mean water velocity in the test section, $V = Q_w/A$, A being the cross-sectional area of the test section, D_o = cylinder diameter, ν = kinematic viscosity of water) was about 3.0×10^3 to 1.8×10^4.

The average bubble diameter was 6.5 mm, with a small standard deviation of 1.35 mm.

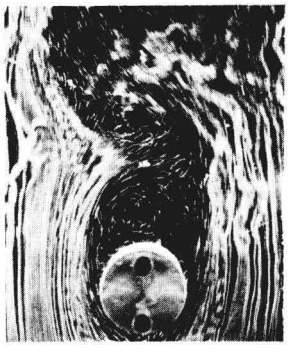

a

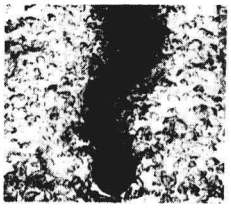

b

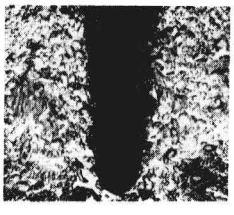

c

Photo 1 (a) Karman vortex shedding in water flow (V=0.4 m/s), (b) Oscillatory wake in two-phase flow (V=0.4 m/s, = 0.06), (c) Steady wake in two-phase flow (V=0.4 m/s, =0.20)